Influence of Operating Conditions and Residual Burned Gas Properties on Cyclic Operation of Constant-Volume Combustion

Quentin Michalski, Bastien Boust and Marc Bellenoue

Abstract The pressure-gain combustion concept is a solution envisioned to increase the thermodynamic efficiency of gas turbines. This article addresses the behaviour of piston-less constant-volume combustion in relevant conditions of engine application. For this purpose, a lab-scale combustion vessel (0.3 L) is run in cyclic operation (10 Hz) with an improved control over the boundary conditions. This facility features the spark-ignited, turbulent combustion of n-decane directly injected in preheated air (423 K, 0.4 MPa), with an overall equivalence ratio of 0.9. Solenoid valves are used to perform the air intake and burnt gas exhaust. A 0D analysis is developed and used to compute the gas thermodynamic evolution based on the experimental pressure traces. The effect of the main operating parameters on the combustion process is discussed: ignition delay, exhaust pressure and wall temperature. The vessel is operated without scavenging, hence the exhaust pressure drives the amount and the temperature of residual burnt gas (16–39% according to the 0D analysis). Highly diluted cycles (exhaust pressure 0.2 MPa) exhibit a higher combustion efficiency, but have a longer combustion duration (3 times more) than those of low dilution (exhaust pressure 0.07 MPa). For a higher wall temperature representative of engine combustor (1000 K), the heat losses are directly reduced, which affects the residual burnt gas properties. This also influences the residual gas temperature (870–1030 K) as well as dilution (10–26%).

Keywords Pressure-gain combustion · Thermodynamic analysis
Cycle optimization

Q. Michalski (✉) · B. Boust · M. Bellenoue
Institut Pprime, (CNRS, ISAE-ENSMA, Universite de Poitiers),
1 Avenue Clement Ader, Teleport 2, BP 40109, 86961 Futuroscope Chasseneuil, France
e-mail: quentin.michalski@ensma.fr

M. Bellenoue
e-mail: marc.bellenoue@ensma.fr

R. King (ed.), *Active Flow and Combustion Control 2018*,
Notes on Numerical Fluid Mechanics and Multidisciplinary Design 141,
https://doi.org/10.1007/978-3-319-98177-2_14

1 Introduction

Future turbomachine generation requires multiple breakthrough to achieve the targets decided for 2050 [1]. Pressure-gain combustion is a direct way to improve the thermal efficiency of aircraft combustor. Different technical solutions are currently developed such as pulsed or rotating detonation, controlled auto-ignition and confined deflagration. The latter, which is referred to as "constant-volume combustion" (CVC) was among the first solutions implemented on ground-based turbomachines through the work of Holzwarth [2]. At the time, large 200 L chambers were fed by an external compressor at 1 to 1.5 bar of initial pressure for a constant-volume combustion working up to 1 Hz with an overall efficiency reported as high as 20% (which is significantly high given the reported operating initial pressure is 1 atm). Recently a simplified prototype of deflagrative chamber with rotating valves, aimed at aircraft application, was operated at higher frequency (25 to 60 Hz) and smaller volume (0.65 L) for improved power density [3] and its combustion stability was investigated [4]. On such device (as on other devices based on deflagration such as wave rotors [5]), a minimum operating frequency is of importance mainly because it reduces the leaks at the clearance gaps between the rotating parts. Regarding the combustor thermodynamic efficiency, several studies discuss the ideal performances of pressure-gain thermodynamic cycles (for detonation as well as for deflagration [5–7]). However few studies performed on real-operated devices discuss non-ideal performances based on energy losses analysis [8]. The pressure rise is intrinsically related to the initial density and dilution of the fresh mixture. For piston-less combustors the exhaust happens at peak pressure and thus follows an adiabatic expansion at constant volume and decreasing mass. The expansion must start directly at the end of combustion. Consequently, the residual burnt gas (RBG) temperature can be considerably higher than that found on four-stroke internal combustion engines (ICE) and close to that found on two-stroke ICE. Since such devices should operate upstream of a turbine, the RBG pressure should also be higher, thus directly affecting the RBG mass (amount and temperature) as well as the expansion ratio. To pursue the investigation of such conditions, a new facility referred to as CV2 was designed. It allows for a simplified operation, a study of performances and a detailed analysis of key processes found in such combustors. Two solenoid valves handle the intake and exhaust, and ensure negligible leaks during combustion. Such choice of technology involves a limited operating frequency (approximately 10 Hz) but allows for a flexible control over cycles time charts. Two dedicated tanks allow for a control over the inlet and exhaust boundary conditions, e.g. exhaust pressure, intake temperature and pressure. Moreover, a 0D multi-zone model is developed to perform the thermodynamic analysis of the experimental combustion cycles. A previous study based on direct injection of gaseous propane evidenced ignition stability issues that were shown to be statistically related to the velocity at ignition [9]. For more representative conditions of practical aircraft combustor application, direct injection (DI) of liquid n-decane is used. Air is preheated up to 423 K and pressure in the chamber is set to 0.4 MPa prior to combustion. In this article, the effect of two crucial boundary

conditions is investigated, namely the exhaust pressure and the wall temperature. Their influence on the thermodynamic efficiency is discussed with respect to the different energy loss phenomena evidenced in the cycle. Selected operating points are optimized and the energy losses related to the different phases of the cycle are compared.

2 Experimental Setup

The CV2 rig is designed to produce cyclic CVC conditions representative of an air-breathing application. The rig is composed of a dedicated intake and exhaust system connected to a single combustion vessel (see Fig. 1). The conditions of intake and exhaust are set in dedicated tanks where the gas composition, pressure and temperature are measured and regulated. Intake and exhaust control systems consist in high-speed valves (COAX MK10) equipped with position sensors (5 kHz). Their response time and transient behaviour were carefully characterized and tabulated (see cross-section in Fig. 4). The thermal load on the exhaust valve, due to burnt gases flowing through, increases its response time. To limit this thermal drift and ensure the repeatability between consecutive sequences, the exhaust valve temperature is regulated at 40 °C (Kistler 2621 F conditioning unit). During an experimental sequence, from the first cycle to the twelfth one, it corresponds to a 3–4 ms maximum delay at opening. The valve is spring-loaded, thus the closing is not affected by the thermal load. Consequently, the exhaust duration is reduced by the same amount of time following the opening delay. This drift is recorded by the position sensors and taken into account in the following analysis. The tanks are connected to the valves through

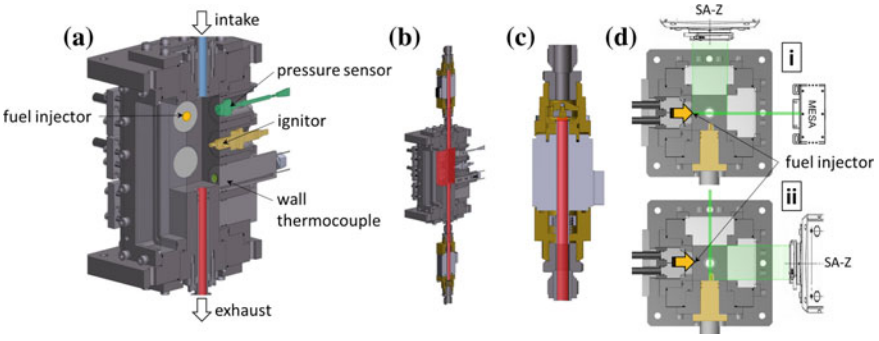

Fig. 1 CV2 in the configuration of interest: **a** combustion chamber and key components; **b** constant-volume parts of the chamber and connections highlighted in red. The wall thermocouple is symmetrically positioned relatively to the cut-plane to the second pressure sensor (in green). **c** High-speed valve where the constant-volume part is highlighted in red. **d** The two configurations (i) and (ii) of the laser sheet and camera: (i) the laser sheet is in the injector symmetry plane, (ii) the laser sheet is in the ignitor plane

flexible hoses of internal diameter 16 mm, length 1 m. The chamber is rectangular with internal dimensions of 50 × 50 × 100 mm. Its aspect ratio λ (length/width) is equal to 2, therefore internal wave dynamics is not as dominant as in wave rotor ($\lambda =$ 13 in [8]). In the present configuration, the closed volume ranges from the intake to the exhaust valve seat, including the connection tubes of internal diameter 12 mm. Overall those volumes account for an additional 0.05 L (see Fig. 1b, c). The complete volume, measured precisely with water, is 0.32 L (0.5% uncertainty) including dead cavities. Intake air is supplied by a 20.76 L (0.3% uncertainty) intake tank at a pressure of 1.0 MPa (0.2% uncertainty). Its volume, including the connecting hose and connecting parts, was precisely measured by weighing the mass variation of a 50 L air bottle while pressurizing the tank. The fuel is injected directly into the chamber through one liquid injector (Bosch 0 261 500 029: 7 holes, 15 ° bias angle) fitted to the wall. The injector is fed with liquid n-decane pressurized at 5.0 MPa. The injector mass flow rate was measured separately, at atmospheric pressure, by weighing the fuel quantity injected for different injection durations, which yields a linearized effective mass flow rate of 6.74 mg per ms of injection (1.1% uncertainty). The initial pressure in the chamber as well as the fuel quantity injected are controlled by varying respectively the intake and injection durations. Ignition is triggered by a non-resistive sparkplug topped with a conventional ignition coil charged up to 2.5 ms (maximum charge), thus delivering an inductive discharge of approximately 40 ± 10 mJ lasting for 2.5 ms. The command, synchronization and acquisition are handled by a National Instrument controller (PXIe-8820 with a PXIe-6363) working up to 100 kHz for fast sensors and 10 kHz for slow sensors. The intake system is thermally insulated and its temperature is regulated by PID-controlled heating collars. The intake hose has its own integrated heating system regulated by its own PID. The chamber is non-insulated and heated with standard cartridge heaters fitted into the walls of the vessel; its temperature is PID-regulated based on the eroding junction thermocouple (Nanmac) used for the local measurement of wall surface temperature. Each experimental sequence is a finite series of twelve cycles. The pressure decrease in the fuel injection tank is negligible, whereas the pressure decrease in the air intake tank is approximately 0.7% per cycle, thus a total 8% of variation for 12 cycles. The overall equivalence ratio (OER) injected during each cycle is kept constant. This is achieved by reducing the fuel injection duration, by a maximum of 1–2 ms from the first cycle to the last cycle depending on the experimental conditions selected. Such variation requires a preliminary calibration of fuel injection duration for each operating point. A broadband oxygen sensor (lambda sensor LSU 4.9) is installed at the exhaust, directly downstream of the exhaust valve. It gives a measurement of the oxygen concentration in the burnt gases and is used to verify that the oxygen concentration found in the exhaust gas matches the one associated with the injected OER. An absolute piezoresistive sensor (Kistler 4049B, 60 kHz bandwidth) is positioned near the oxygen sensor for transient pressure recording. This measurement is used to compensate the lambda measurement as the exhaust pressure varies [10]. A piezoelectric sensor (Kistler 6067C, 90 kHz bandwidth) is used for pressure recording in the combustion vessel. A silicon layer is deposited on its surface, approximately 1 mm thick, to prevent thermal drift. For combustion

pressure measurement, an absolute piezoresistive sensor (Kistler 4049B) is used in the chamber as well to compensate for the piezoelectric thermal drift. Those two sensors are temperature-regulated (70 °C) by a dedicated Kistler 2621 F conditioning unit. The OER is computed by measuring the pressure variation in the air tank for each cycle and by the a priori calibration of the injector mass-flow rate. Using the perfect gas law and assuming isentropic expansion in the air tank, the OER of the fresh charge introduced in the chamber during the cycle reads

$$OER = D_{st} \frac{\gamma_a m_f}{M_a \Delta p_a V_a} \tag{1}$$

where M, Δp, m and V are respectively the molar mass, pressure variation, mass variation and tank volume, a and f stand respectively for air and fuel tanks and D_{st} is the mass air-fuel ratio of a n-decane air stoichiometric mixture. The injection of both air and fuel starts after the closing of the exhaust valve, that way there is no scavenging phase. The effective OER in the chamber thus corresponds to the injected OER. The uncertainty in the OER for one cycle is mainly related to the air tank pressure measurement, Δp (16 mbar of uncertainty). However, given the high reproducibility of the valve opening cross-section (measured optically), one can suppose the linearization of the pressure loss starting from the third cycle. Doing so, the uncertainty in Δp for a single cycle drops to 5.4%, which yields an uncertainty of 6.8% in the OER calculated for a single cycle, e.g. at OER = 0.9, it corresponds to an uncertainty of 0.06. 2D time-resolved particle image velocimetry (PIV) is performed to characterize the aerodynamic conditions. The air injected in Fig. 2b was oil-seeded (2.0 μm SMD), which can be seen in the first image (SOI+0.2 ms). As for Fig. 2a, air was not oil-seeded although residual particles can be seen in the air flow. Additionally, Mie tomography pictures give an insight into the fuel atomization during the intake phase. PIV is performed at 20 kHz (50 μs time between two velocity fields), which means the laser emission (Nd:YAG, 532 nm MESA PIV) works at 20 kHz and the camera (SA-Z Photron) works at 40 kHz. To account for the velocity variation encountered in one cycle, a variable PIV interframe delay (from 2 μs to 25 μs) is used (PTU X from Lavision). The filling process is highly repeatable and the interframe profile is tuned after a few iterations on experiments. PIV data is processed with a multi-pass iterative calculation starting from 64 × 64 px down to 16 × 16 px with a 50% overlap (Davis 8.4.0). This yields a physical velocity resolution of 1.3 × 1.3 mm.

The PIV velocity fields highlight an internal aerodynamics structured around a highly compressible flow which penetrates the chamber a few milliseconds after the opening of the valve and generates intense shear flow on the walls [11]. Air and fuel are injected simultaneously for enhanced mixing and atomization (see Fig. 2) during a fully closed exhaust phase. The injection process is apparently delayed, due to the time induced by the 150 mm distance from the valve seat to the chamber. The same delay occurs after the closing of the valve, as flow is still observed on the pictures. Finally the velocity decay is exponential because of a free-turbulence decay during this later phase. Regarding the atomization process, the PIV yields intake velocities of

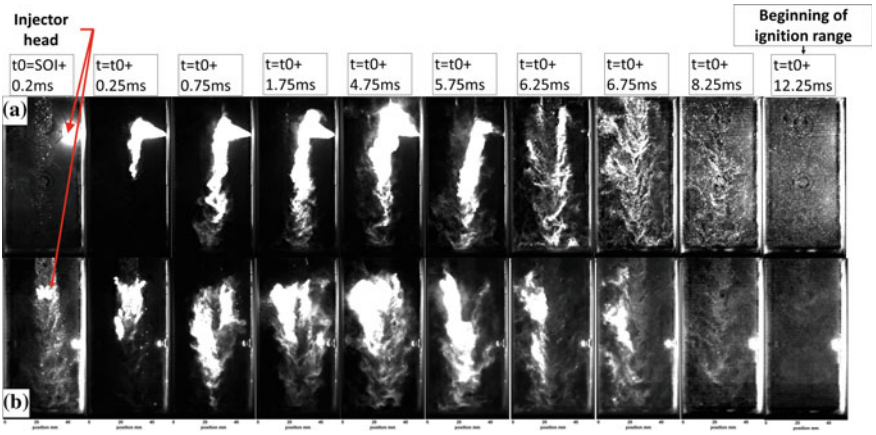

Fig. 2 Mie tomography images of the intake phase during a reactive combustion cycle, which shows the atomization of the spray on the main air mass flow from the centre upper part of the chamber. A. PIV in injector plane (see Fig. 1a), B. PIV in ignitor plane (see Fig. 1b)

approximately 250 m/s (confirmed by LES [11]) at air mass flow rates ranging from 60 to 75 g/s. Phase-Doppler interferometry (PDI) measurements were performed on a cold injector (21.5 °C) fueled with n-decane outside the chamber at ambient conditions, using an Artium PDI-200MD equipped with focal lenses of 500 mm for both emission and reception (1.6–180 μm detection range). Those measurements performed 30 mm downstream of the injection head yield an average droplet velocity of 18.5 m/s and a 30 μm Sauter Mean Diameter (SMD), for a mass flow rate of 6.74 g/s. The fuel spray and the air are injected simultaneously. Obviously, the spray and the central air plume have a similar dimension at their impingement point. This behaviour prevents the fuel spray to reach the wall and promotes a uniform distribution of the fuel droplets in the chamber (as seen on the last MIE tomography pictures of Fig. 2). Regarding this spray-air plume interaction, based on a fuel density of 643 kg/m3 (403 K and 1 bar), an air viscosity of 24.1 μPa.s (423 K and 1 bar), the fuel particles are estimated to penetrate up to 0.1 mm into the air plume which corresponds to 1 % of its total width [12]. Along their trajectory, the droplets evaporate so that the penetration length should then be lower. Such behavior is thus consistent with the Mie tomography pictures recorded for PIV measurements during the simultaneous fuel and air injection (Fig. 2). In the following, the procedure for the 0D calculation fit to the acquisition is detailed.

3 0D Numerical Setup

A specific 0D multi-zone code was developed to compute the time-resolved evolution of non-directly measurable properties such as mixture density, exhaust gas temperature and composition. The code is developed under Matlab R2015b. The chemical

description of the fluid is based on the Cantera (2.3.0) Matlab library [13] using a reduced number of species to speed up the computation. The species included in the description are $H_2, O_2, OH, H_2O, CO, CO_2, NO, N_2, nC_{10}H_{22}$ which thermodynamic properties are taken from standard JANAF table. The model includes a separate representation of each vessel with regard to heat or mass transfer, including the intake tank and line (AD), the fuel injection tank (INJ T), the combustion chamber (CC), the exhaust tank (EJ) and the exhaust line (EJL) (Fig. 3). The isochoric combustion phase is modeled through a three-zone description. Combustion happens in 3 phases: the flame propagates over a slice of fresh gases, this reacting slice (referred to as zone 13 in Fig. 3) is set to chemical isobaric equilibrium at fixed enthalpy, which increases its volume. The overall volume of gas in the chamber is temporarily higher than the geometrical chamber volume. The 3 volumes of gas in the chamber are compressed (without mixing) at fixed entropy until their cumulated volume matches the chamber volume. At each integration step, the burning slice (zone 13 see Fig. 3) is mixed with the burnt gases (zone 12 see Fig. 3). The combustion duration is set as measured from experimental data for each cycle. Unburnt gases are accounted for by stopping the combustion over a volume including the gaps of the chamber assembly, as well as the quenching distance estimated at 100 µm according to high-pressure measurements [14]. Overall unburnt gas accounts for 3.0% of the total volume with 2% due to the cavity quenching and the remaining 1% due to the flame-wall quenching. At the end of the combustion phase, fresh gases and burnt gases are mixed, thus the chemistry is frozen during the exhaust phase until the combustion of the following cycle. For each cycle, the intake and exhaust durations are set as measured on their respective position sensors. The intake flow is choked during most of the

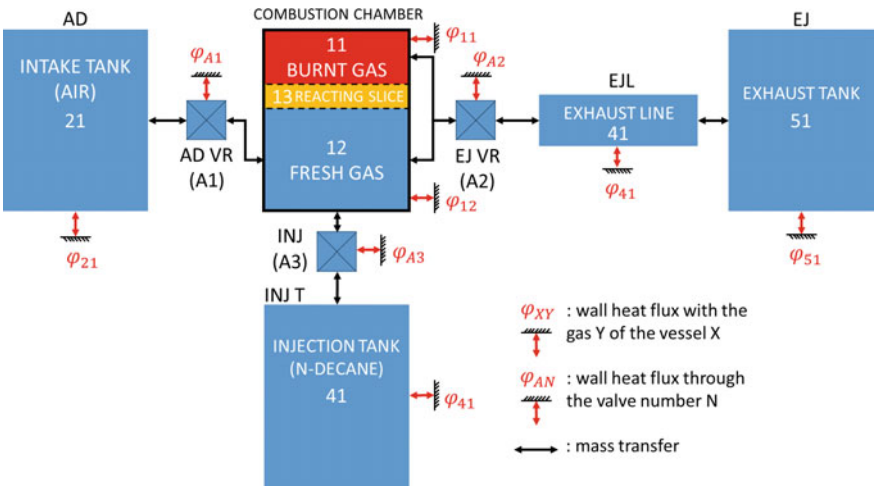

Fig. 3 Graphical description of the vessels described in the 0D analysis with detailed number of heat (ϕ with index relative to the gas phase number, red arrows) and mass transfer (black arrows) connections set between the vessels

intake phase, a constant discharge coefficient is thus set until the mass drop measured experimentally in the intake tank matches the 0D simulated one that sets the mass of air injected per cycle into the chamber. During the first cycle, the sensible enthalpy loss is set for the air that flows through the valve (which internal temperature is lower than the pre-heated air) until the initial pressure in the chamber is matched. Wall heat transfer coefficient h (in $W/m^2/K$) is modeled using Hohenberg's correlation [15]

$$h = 130 V_{cc}^{-0.06} p_{1X}^{0.8} T_{1X}^{-0.4} (v + 1.4)^{0.8} \tag{2}$$

where V_{cc} is the volume of the chamber, p_{1X} and T_{1X} are the pressure and temperature of the gas phase for $X = 1$ or 2 (either fresh or burnt gases). The representative velocity v is computed based on the chamber cross-section and on the instantaneous mass-flow rate. The experimental increase in wall temperature is less than 10 K during combustion (see Fig. 4); there is enough time for heat conduction between each cycle, so that the cumulated wall temperature rise at the end of the 12th cycle is of 28 K. The wall temperature for the 0D calculation is thus considered constant over a complete sequence. The overall pressure shape is matched for the combustion phase and the exhaust phase on most cycles by adjusting the velocity (during the

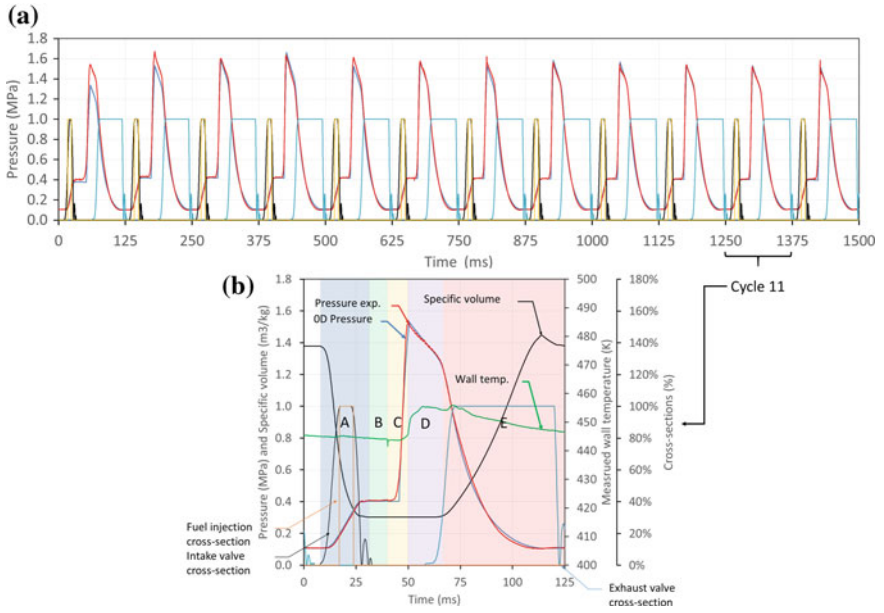

Fig. 4 **a** Comparison between numerical 0D pressure (in blue) and experimental pressure signal (in red) for a single sequence (12 cycles) with intake (black), fuel injection (orange) and exhaust (blue) cross-sections. **b** Best fitted cycle selected for detailed analysis, the specific volume is figured as well. The different phases of the experimental cycle are figured in color (A the intake, B the relaxing phase, C the combustion, D the isochoric cooling and E the exhaust). The wall temperature is figured in green

combustion and the isochoric cooling phase) and the exhaust discharge coefficient. Only experimental conditions with consecutive successful ignitions are analyzed. In the present cases, the cycle-to-cycle variation is low enough so that one cycle can be considered as representative of the whole set.

4 Detailed Analysis on One Operating Point

More details are given on the comparison between the experimental pressure signal and its respective computed 0D value.

The pressure signal is well matched during the intake phase until the opening of the exhaust (Fig. 4). The exhaust is more complex to simulate for several reasons. First the flow is only choked for part of its duration and the stagnation pressure and temperature vary during the exhaust phase. Also, the temperature of the exhaust gas, higher than that of the intake, increases the volume flow rate. Even with the large exhaust pipes (16 mm inner diameter), the pressure rises slightly in their residual volume. This effect is accounted for by using an intermediate volume EJL between the exhaust tank and the chamber. The unburnt gas influence is quantified as follows. From the conditions of Fig. 4b cycle, the unburnt volume is varied from 0 to 6.0%. The mass fraction of unburnt gas depends on the maximum pressure reached. At 3.0% unburnt volume, up to 8.7% of the end-compression gases remain unburnt which accounts for a 0.10 MPa straight pressure loss (reference value of 0 MPa in Table 1). If this unburnt volume is brought to 0%, the resulting maximum pressure is thus raised by 0.1 MPa (hence with a positive sign in Table 1). Such unburnt volume can indeed be avoided by optimizing the chamber design. The assembly gaps (required in our modular conception) can be avoided in the case of real application designs, possibly made by additive manufacturing. As well, fuel-charge stratification can limit the effect of flame-wall interaction by isolating the combustion in the centre of the chamber, thus reducing the amount of unburnt gas due to quenching.

A constant value of 3.0% of unburnt gases in volume (among which 1.0% is due to quenching distance) corresponding to our estimation is considered in the following analysis. Once properly tuned, from one sequence to another with different experimental settings, e.g. varying exhaust pressure or ignition timing, only small adjustments to the heat transfer model parameters are made to match the pressure traces. The heat lost to the wall is then compared to the ideal heat of combustion $Q_c = \Delta m_f I_p$, with $I_p = 44.2$ MJ/kg being the lower heating value of n-decane. During

Table 1 Effect of unburnt gases on the maximum pressure, the reference volume values are in bold

Percentage of unburnt volume (%)	0	**3.0**	6.0
Unburnt mass (%)	0	**8.7**	16.5
Induced relative pressure variation (MPa)	+0.10	**0**	−0.09

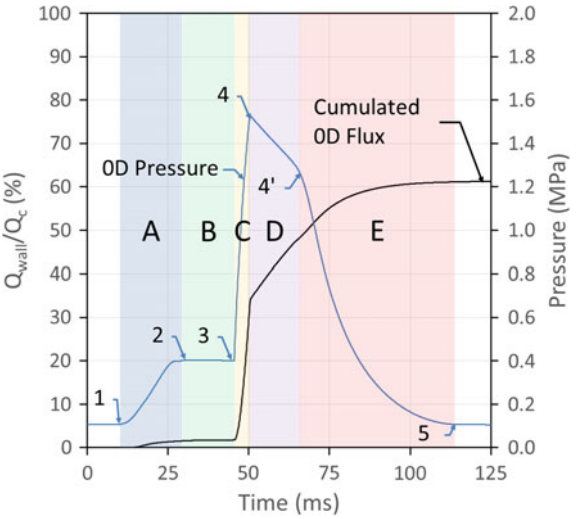

Fig. 5 Experimental and 0D simulated cumulated wall heat flux Qw in percentage of Qc, with its respective 0D pressure signal used to figure the different phases of the 0D cycle. The reference points (1, 2, 3, 4, 4' and 5) for energy losses calculation during each phase are figured

the intake phase, turbulent mixing occurs between the RBG and the fresh gases. This partially premixed charge of RBG, air and fuel, is continuously cooled by the walls at a rate driven by near-wall turbulence. A fraction of the total thermal energy (2.0% in Fig. 5) is thus lost during the intake phase (A-B). Approximately 30% of Q_c is transferred to the wall during the combustion phase (C), 18% after the combustion is complete and before the exhaust full opening (D), and 11% during the exhaust phase (E) until the pressure equilibrium is completed. Indeed, those values depend on the unburnt volume taken in the computation. Considering the wall heat flux is adjusted to match the pressure peak, a lower unburnt mass fraction would require a higher wall heat flux and vice-versa. Nevertheless, the same amount of energy-loss must be set to match the pressure.

The intake phase (A) starts at point 1 and ends at point 2. Following a relaxation phase (B) which duration depends on the chosen ignition timing, the isochoric combustion phase (C) then starts from point 3. On that cycle, the maximum combustion pressure reaches 1.53 MPa at point 4. The beginning of the exhaust phase is delayed to make sure the whole combustion process is isochoric. Therefore, the combustion phase is followed by a 25 ms isochoric cooling phase that comprises a true isochoric phase as well as part of the unsteady opening of the valve (approximately 15 ms). The isochoric cooling phase (D), from 4 to 4', is a straight energy loss whereas the exhaust phase (E) is a non-adiabatic expansion that starts from 4' to pressure equalization with the exhaust tank. A post-processing is made from the condition 3, to compute the associated ideal isochoric and adiabatic combustion. Under constant heat capacity and perfect gas assumptions, the adiabatic pressure ratio π_a is directly related to the energy-loss and computed as:

$$\pi_a = \frac{p_4 - p_3}{p_{4a} - p_3} \tag{3}$$

Table 2 Cycle thermodynamic properties and detailed balance of energy losses. The dilution is given in mass percentage relative to the mass at ignition

	Unburnt volume (%)	Maximum pressure (MPa)	RBG Dilution (%)	Residual temperature before intake (K)	Temperature after intake (K)
Cycle properties	3.0	1.53	22.0	500	434
	Intake losses	Unburnt gases	Combustion losses	Isochoric cooling heat losses	Exhaust heat loss
Energy loss Q/Q_c (%)	1.8	8.7	32.4	12.6	14.5

where p_{4a} is the adiabatic and isochoric combustion pressure. In Fig. 5, this pressure ratio is 67% which is consistent with the 41 % energy-loss simulated during the combustion phase from point 3 to 4 (see Table 2): 8.7% corresponding to unburnt gases and 32.4% to heat losses. In the following, this energy-loss balance is used to evaluate the effect of initial conditions (at point 3) on combustion through RBG dilution, both in mass and temperature. At fixed boundary conditions, the influence of the ignition timing is discussed by combining experiments and 0D simulation analysis.

5 Influence of the Ignition Timing on the Cycle Performances

To improve the power density, high operating frequency is required. Consequently, combustion cycles need to be as short as possible. For combustion to be as fast as possible after ignition, one requires both high turbulence as well as favourable local mixture conditions in equivalence ratio and dilution to promote ignition success and flame velocity. The local variation of those properties has a direct impact on the ignition probability and on the ignition kernel growth towards the rest of the chamber. A previous study in direct gaseous injection with non-preheated air evidenced the sensitivity of ignition success to the local velocity properties; for a given dilution and equivalence ratio, statistical limits for the velocity were evidenced [9]. Only stable conditions are considered in the following. For that purpose, the overall equivalence ratio selected is 0.90 ± 0.05, and the exhaust backpressure is set to 1 bar to limit the RBG dilution to approximately 20%. The ignition timing is varied from the end of the intake phase, to 15 ms later (12% of total cycle duration).

During that time, the mean velocity in the chamber drops from approximately 50 m/s, at the beginning of the pressure plateau, to 15 m/s in 3 ms, at the end of the first rebound, and then decays from 15 m/s to less than 5 m/s in the following

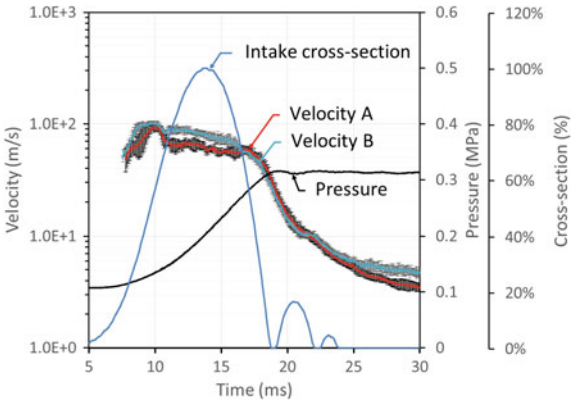

Fig. 6 Ensemble-averaged mean velocity in the chamber (with the cycle-to-cycle standard deviation as bars) from two separate sequences, for a PIV plane on the injector head (red) and in front of the injector head (blue). A and B refers to the cases presented on Fig. 2. The intake cross-section and pressure signal are figured as well. The initial pressure is slightly lower (3.2 MPa) than for the rest of the studied sequences (4.0 MPa) which affects the velocity magnitude but not the timings of events

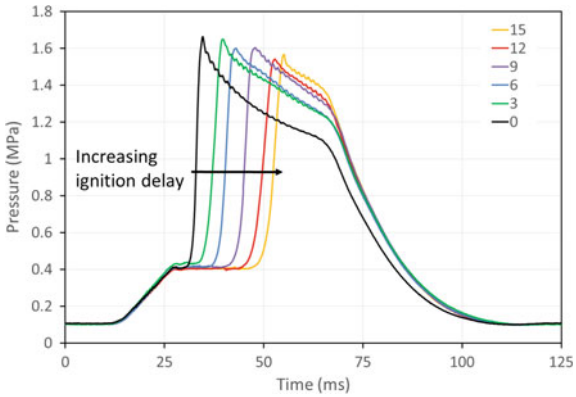

Fig. 7 Instantaneous experimental pressure signals for different cycles with varying ignition timing relative to the beginning of the pressure plateau (closing of the intake valve)

10 ms (Fig. 6). At OER = 0.9, the ignition timing is varied from the beginning of the pressure plateau to 15 ms by step of 3 ms (Fig. 7).

Characteristic combustion durations based on the pressure signal are usually computed to describe the different phases of the combustion process. Those durations are defined based on a percentage of the non-adiabatic combustion pressure gain, π, between the pressure at ignition and the maximum combustion pressure reached:

$$t_X = t(\pi = \frac{p_x - p_3}{p_4 - p_3} = X\%) \tag{4}$$

$$t_{X-Y} = t_Y - t_X \tag{5}$$

Table 3 Combustion characteristic average times with their respective standard deviation given for varying ignition delays as well as RBG dilution properties

Ignition delay	15 ms	12 ms	9 ms	6 ms	3 ms	0 ms
t_{0-10} (ms)	7.4 ± 0.6	6.8 ± 0.4	6.5 ± 0.4	5.5 ± 0.4	4.7 ± 0.5	3.3 ± 0.6
t_{10-90} (ms)	4.2 ± 0.4	3.8 ± 0.6	3.4 ± 0.2	2.9 ± 0.2	2.7 ± 0.3	1.8 ± 0.5
t_{90-100} (ms)	1.5 ± 0.4	1.3 ± 0.3	1.2 ± 0.4	1.1 ± 0.4	0.7 ± 0.4	0.7 ± 0.2
RBG Temperature (K)	527	514	512	497	486	460
RBG Dilution (%)	21.4	21.7	22.0	22.4	22.2	23.0
p_4 (MPa)	1.54	1.52	1.59	1.59	1.61	1.66
Expansion ratio (-)	12.8	12.4	11.9	11.4	11.2	10.5

According to these formulas, the duration t_{0-10} can be considered as representative of the time taken for ignition kernel growth to free flame propagation, t_{10-90} corresponds to free flame propagation and t_{90-100} corresponds to the end of propagation at which the flame-wall interaction is maximum (Table 3).

For every ignition timing, the exhaust timing is kept constant. The overall combustion duration is strictly decreasing (reduced by almost a factor of 2) towards earlier ignition timing. At a given OER and almost constant RBG dilution rate, the flame velocity depends on the turbulent velocity fluctuation, in first-order approximation [3, 16]. At the closing of the intake valve, turbulent velocity rapidly decays following the mean velocity evolution (Fig. 6). Earlier ignition yields higher flame velocity, which thus results in shorter combustion duration. The following isochoric cooling phase duration then increases for earlier ignition, which in turn increases the heat losses. The consequence is a lower initial pressure for the exhaust expansion, which can be seen directly on the pressure signal (Fig. 7). At the earliest ignition timing (0 ms), 33% of the fuel energy is lost to the wall during the isochoric cooling phase. Those losses drop to 8.6% for the latest ignition (15 ms). As the peak combustion pressure is almost the same (1.54 MPa at 15 ms to 1.66 MPa at 0 ms), the more cooling there is during that phase, the lesser the initial exhaust pressure, the less efficient the cycle will be by lowering the potential for work recovery. However, higher initial pressure prior to expansion means higher velocity and temperature at the opening of the exhaust valve, which yields slightly higher heat losses during the exhaust phase. Considering any actuator used to control the isochoric phase will have their own time response, a trade-off must be found between the isochoric cooling phase losses and a fully isochoric combustion for optimal work recovery. Following Fourier's law, in first-order approximation, the heat losses are directly related to the wall temperature. The rig is not designed to reproduce stationary thermal equilibrium conditions. Therefore, the wall temperature is much lower than what could be expected in indus-

trial applications, hence higher heat losses. In the following, we discuss the influence of the boundary conditions on the combustion properties through an experimental variation of the exhaust pressure. The effect of the wall temperature is also discussed through the 0D simulation.

6 Influence of the Boundary Conditions on Experimental Cycle Performances

In turbomachines, the combustor backpressure is a design parameter that can be controlled by the cross-section of the turbine first stage diffuser. Turbine efficiency is related to its pressure expansion ratio, and choked conditions are usually set at the first stage diffuser for best efficiency. In piston-less CVC processes, the exhaust back-pressure directly drives the expansion ratio from the pressure at the beginning of the exhaust (point 4'), to the exhaust backpressure (point 5). The expansion ratio, in turn, affects the RBG density through the resulting pressure and temperature at the end of exhaust phase. The operating points experimentally investigated start at an initial pressure of 4.0 MPa for a constant OER = 0.9. With increasing backpressure, an increased mass of RBG is trapped into the chamber and a lower air mass is introduced into the chamber. This is achieved through a reduction in intake valve opening duration (1 ms of opening corresponds to an increase of 250 mbar). The energy density is thus reduced for higher backpressure. The ignition timing (12 ms) as well as the exhaust opening duration are kept the same (see Fig. 8). Under those conditions, the higher the dilution, the slower the combustion, so that combustion duration is affected by a factor of 2.8 between an exhaust pressure of 0.07 MPa and 0.21 MPa (Table 4). Given the exhaust valve is opened at the same timing for each operating point, the isochoric cooling phase is long enough for each operating point

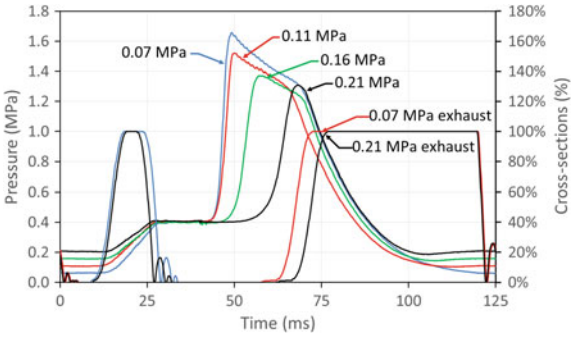

Fig. 8 Experimental pressure signals of single cycles with the same ignition timing (12 ms) for the 4 different backpressure investigated, 0.07 MPa (blue), 0.11 MPa (red), 0.16 MPa (green) and 0.21 MPa (black). The two extreme traces of intake (imposed) and exhaust (thermal drift) cross-sections are represented following the colour code as the one for their associated backpressure

to have the same initial exhaust expansion pressure (1.3 MPa). The expansion ratio decreases with the exhaust pressure from 18 to 6.3, hence higher temperature for higher exhaust backpressure. The trapped residual mass is influenced by the residual density through the expansion ratio and the initial exhaust pressure. Under those conditions, the exhaust gas quantity increases by 16.6% in mass every 0.1 MPa of backpressure. The fundamental flame velocity is known to decrease with increasing dilution (see [17]) for experimental measurements on diluted iso-octane/air flame) and to increase with the temperature. However, considering the important cooling of the exhaust gases, both during combustion (Fig. 9) and exhaust (Table 4), the increase in initial temperature (after mixing with the fresh mixture) is not high enough to compensate for the increase in dilution, hence a lower fundamental flame velocity. The energy density for diluted cycles is lower. They exhibit lower maximum pressure, and slightly lower combustion temperatures. The final density in the fresh gas when combustion stops (see point 4 on Fig. 5) is thus lower, which yields a reduced unburnt mass fraction and a higher combustion efficiency. In the present experiments, the heat losses are high because of the low wall temperature (423 K). In turbojet engines, the thermal management of the combustor is based on compressed air bypassed from the compressor stages. That means higher working temperatures are envisioned. The same cycle is simulated keeping the heat loss coefficient, combustion duration (as the real duration is difficult to estimate) and intake gas temperature constant, but at a wall temperature of 1000 K (which is compatible with most Inconel alloys). This lowers the combustion losses by 10% and isochoric cooling phase losses by a few percent (at which the temperature difference is maximum). The temperature of the cycle is overall higher, heat is gained by the charge during the intake, and the heat losses during the exhaust are lower, hence a higher initial temperature (Table 5). The flame velocity should thus be higher, which should reduce the heat losses during combustion (as seen with the variation of ignition timing). The increase of wall temperature increases the gas temperature in each phase of the cycle. In the present conditions, an increase of the exhaust pressure yields spontaneous re-ignition during fuel injection

Table 4 Combustion characteristic conditions (exhaust expansion ratio, RBG dilution of the mixture, the initial residual temperature, initial temperature of the cycle fresh mixture) and average times with their respective standard deviation given for varying backpressure

Exhaust backpressure	0.21 (MPa)	0.16 (MPa)	0.11 (MPa)	0.07 (MPa)
Wall temperature (K)	423			
Dilution (%)	38.7	31.3	22	15.8
Expansion ratio (-)	6.3	7.9	12.3	18
Residual temperature (point 5) (K)	577	547	500	469
Initial temperature (point 2) (K)	439	436	434	436
t_{0-10} (ms)	14.1 ± 1.1	10.2 ± 1.1	6.7 ± 0.6	5.1 ± 0.3
t_{10-90} (ms)	7.3 ± 0.6	5.4 ± 0.6	4.0 ± 0.6	2.7 ± 0.3
t_{90-100} (ms)	2.6 ± 0.7	2.2 ± 0.7	1.2 ± 0.6	0.8 ± 0.6

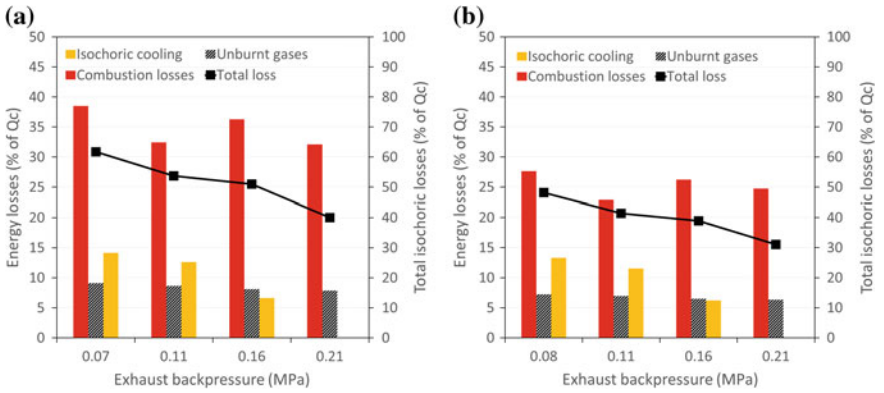

Fig. 9 **a** Energy balance during the combustion phase with heat losses (coloured background) and unburnt gas losses, for 4 different backpressures corresponding to the experimental boundary conditions ($T_w = 423$ K). **b** Same energy balance for a 0D simulation at $T_w = 1000$ K

[18]. This behaviour is closely related to the RBG temperature, hence spark-ignited cycles operating at wall thermal equilibrium conditions would certainly evidence such phenomena. Moreover, it would start at a lower exhaust backpressure, since the vessel is operated without scavenging. In other pressure-gain combustion applications, this behaviour is also under consideration, in order to avoid pre-ignition in high-frequency PDE (relative to spark-ignition) [19] or to control it in pulsed combustor [20]. The optimization of such cycles requires the reduction of the isochoric cooling phase duration to a minimum. This requires an optimization of the opening of the exhaust valve. An early opening of the exhaust valve yields a truncated pressure at the end of combustion which is then isobaric (although occurring at final pressure). For an ignition timing of 3.0 ms (Table 3), an optimization is made on the exhaust timing (Fig. 10a). The cycle duration is adjusted (reduced by 25 ms) to avoid further heat losses after the expansion, while still avoiding scavenging. For the two compared cycles (Fig. 10a), the OER (0.87) is the same with a slightly higher initial pressure for the unoptimized cycle (0.43 MPa) compared to the optimized cycle (0.40 MPa). In both cases, the dilution is identical (0.3% difference). With the optimization, the isochoric cooling phase is shorter, resulting in a 3.4% isochoric cooling loss compared to 21.0% for the unoptimized cycle. As the pressure ratio is higher, the mass flow rate increases, hence higher exhaust velocities that result in higher heat fluxes. The same optimized cycle is processed with an increased 1000 K wall temperature (same as Fig. 9b). Doing so, the combustion heat losses are 9% lower, the unburnt gas mass is 2% lower; but as for unoptimized conditions, the heat losses during the isochoric phase remain the same. Working in partially premixed conditions, the burnt gases at the end of combustion are directly exposed to the chamber walls, hence a high temperature gradient (still approximately a 1000 K difference) once the flame

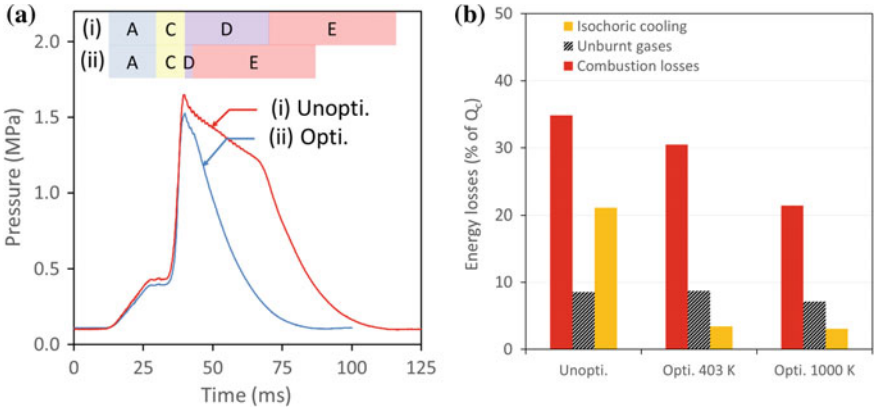

Fig. 10 **a** Comparison of experimental pressure signals for a cycle with optimized cycle (blue), with almost no isochoric phase and shorter cycle duration (100 ms instead of 125 ms) and unoptimized cycle (red). The different phases for the two cycles are figured as in Fig. 5. The ignition timing being early (at 31 ms), there is no relaxation phase" **b**

Table 5 Combustion characteristic conditions (exhaust expansion ratio, RBG dilution of the mixture, the initial residual temperature, initial temperature of the cycle fresh mixture) for the extrapolation at $T_w = 1000$K

Exhaust backpressure	0.21 (MPa)	0.16 (MPa)	0.11 (MPa)	0.07 (MPa)
Wall temperature (K)	1000			
Dilution (%)	26.4	20.7	13.8	10.2
Expansion ratio (-)	7.2	9.3	15	21.1
Residual temperature (point 5) (K)	1028	975	911	871
Initial temperature (point 2) (K)	756	708	677	652

reaches the wall, which yields high heat flux. Such behaviour can be avoided by using a convenient air-fuel stratification strategy similar to spark-ignited ICE, where the mixture is fuel-rich at the centre of the cylinder and fuel-lean near the walls.

7 Conclusion

A constant-volume combustion chamber is operated with pre-heated air (423 K at an initial pressure of 0.4 MPa) and a directly injected liquid n-decane with a cyclic operation reaching up to 12 cycles. The combustion characteristics are shown to be strongly dependent on the residual burnt gas properties. Those properties are influenced by the two main boundary conditions of the cycle, namely the exhaust pressure and the wall temperature. In the current setup, the walls are heated up to 423 K which is sufficient to prevent the condensation of n-decane but is far too low

to be representative of thermal equilibrium, thus allowing for an important cooling of the burnt gases. The expansion ratio is varied by a factor of 3 mostly by varying the exhaust backpressure. With higher backpressure, the dilution as well as the RBG temperature are increased. Nevertheless, due to an important cooling of those burnt gases during the exhaust phase, and due to the addition of the fresh charge, the resulting initial temperature is not affected. This results in a slower combustion, as the characteristic combustion time increases by a factor of 2.8 as the RBG dilution increases from 15.8% to 38.7%. In the case of a higher wall temperature, the cooling of RBG is reduced hence an increased temperature and a reduced mass fraction of residual burnt gases. As a result, the initial gas temperature increases with increasing exhaust backpressure. Among the losses which are accounted for on the present device, a certain amount is expected to be easily reduced further in an industrially designed chamber. Premixed combustion in internal combustion engines leads to higher heat losses as the burnt gases and the flame are directly in contact with the walls. Stratified combustion would thus help reduce both the heat losses during the combustion and the unburnt gas generated by quenching to the walls and inside mechanical gaps; hence leading to higher combustion efficiency.

Acknowledgements This work is part of the CAPA Chair research program on Alternative Combustion modes for Air-breathing Propulsion supported by SAFRAN Tech, MBDA France and ANR (French National Research Agency).

References

1. European Commissio: Flighpath 2050—Europe's Vision for Aviation (2011). https://doi.org/10.2777/50266
2. Holzwarth, H.: The gas turbine: theory, construction and records of the results obtained from two actual machines (1912)
3. Boust, B., Michalski, Q., Bellenoue, M.: Experimental investigation of ignition and combustion processes in a constant volume combustion chamber for airbreathing propulsion. In: AIAA (2016). https://doi.org/10.2514/6.2016-4699
4. Labarrere, L., et al.: Experimental and numerical study of cyclic variations in a constant volume combustion chamber. Combust. Flame **172**, 49–61 (2016). https://doi.org/10.1016/j.combustflame.2016.06.027
5. Akbari, P., Nalim, M.R., Donovan, E.S., Snyder, P.H.: Leakage assessment of pressure-exchange wave rotors. J. Propul. Power **24**(4) (2008). https://doi.org/10.2514/1.31725
6. Zockel, M.: The constant volume gas turbine—a thermodynamic assessment. In: ASME (1974)
7. Wintenberger, E., Shepherd, J.E.: Thermodynamic cycle analysis for propagating detonations. J. Propuls. Power **22**(3), 694–698 (2006). https://doi.org/10.2514/1.12775
8. Nalim, M.R., Snyder, P.H., Kowalkowski, M.: Experimental test, model validation, and viability assessment of a wave-rotor constant-volume combustor. J. Propuls. Power **33**(1) (2017). https://doi.org/10.2514/1.B36174
9. Michalski, Q., Boust, B., Bellenoue, M.: In Revision. Experimental investigation of ignition stability in a cyclic constant-volume combustion chamber featuring relevant conditions for air-breathing propulsion. Flow Turbul Combust
10. Asad, U., Tjong, J., Zheng, M.: Exhaust gas recirculation—zero dimensional modelling and characterization for transient diesel combustion control. Energy Convers. Manag. **86**, 309–324 (2014). https://doi.org/10.1016/j.enconman.2014.05.035

11. Michalski, Q. et al.: Joint numerical and experimental characterization of the turbulent reactive flow within a constant volume vessel. In: AIAA JPC (2018)
12. Rudinger, G.: Penetration of particles injected into a constant cross flow. AIAA J. **12**(8), 1138–1140 (1974). https://doi.org/10.2514/3.49429
13. Goodwin, D.G., Moffat, H.K., Speth, R.L.: Cantera: An object-oriented software toolkit for chemical kinetics, thermodynamics, and transport processes. Version 2.3.0. (2017). http://cantera.org
14. Labuda, S., Karrer, M., Sotton, J., Bellenoue, M.: Experimental study of single-wall flame quenching at high pressures. Combust. Sci. Tech. **183**(5), 409–426 (2010). https://doi.org/10.1080/00102202.2010.528815
15. Hohenberg, H.: Advanced approaches for heat transfer calculations. SAE Tehnical Paper, Issue 790825 (1979). https://doi.org/10.4271/790825
16. Lipatnikov, A.N., Chomiak, J.: Turbulent flame speed and thickness: phenomenology, evaluation, and application in multi-dimensional simulations. Prog. Energy Combust. Sci. **28**, 1–74 (2002)
17. Endouard, C., Halter, F., Chauveau, C., Foucher, F.: Effect of CO2, H2O, and exhaust gas recirculation dilution on laminar burning velocities and markstein lengths of iso-octane/air mixtures. Combust. Sci. Tech. (2016). https://doi.org/10.1021/ef101482d
18. Michalski, Q., Boust, B., Bellenoue, M.: Toward a cyclic self-ignited constant-volume combustion for airbreathing propulsion applications. In: AIAA—Joint Propulsion Conference (2018)
19. Mastuoka, K., Takagi, S., Kasahara, J.: Validation of pulse-detonation operation in low-ambient-pressure environnement. J. Propuls. Power **34**(1), 116–124 (2018). https://doi.org/10.2514/1.B36401
20. Yungster, S., Paxson, D.E., Perkins, H.D.: Effect of fuel injection and mixing characteristics on pulse-combustor performance at high-pressure. In: AIAA Propulsion and Energy Forum (2014). https://doi.org/10.2514/6.2014-3728